

Performance of the Southern African Large Telescope (SALT) High Resolution Spectrograph (HRS)

Lisa A. Crause^{*a}, Ray M. Sharples^b, David G. Bramall^b, Jürgen Schmoll^b, Paul Clark^b, Eddy J. Younger^b, Luke M. G. Tyas^c, Sean G. Ryan^d, Janus D. Brink^c, Ockert J. Strydom^c, David A. H. Buckley^c, Martin Wilkinson^c, Steven M. Crawford^a, Éric Depagne^c

^aSouth African Astronomical Observatory, P.O. Box 9, Observatory 7935, Cape Town, South Africa

^bDurham University, Centre for Advanced Instrumentation, Department of Physics, Science Laboratories, South Road, Durham, DH1 3LE, United Kingdom

^cSALT Foundation, P.O. Box 9, Observatory 7935, Cape Town, South Africa

^dUniversity of Hertfordshire, Hatfield, Hertfordshire, AL10 9AB, United Kingdom

ABSTRACT

The Southern African Large Telescope (SALT) High Resolution Spectrograph (HRS) is a fibre-fed R4 échelle spectrograph employing a white pupil design with red and blue channels for wavelength coverage from 370–890nm. The instrument has four modes, each with object and sky fibres: Low (R~15000), Medium (R~40000) and High Resolution (R~65000), as well as a High Stability mode for enhanced radial velocity precision at R~65000. The High Stability mode contains a fibre double-scrambler and offers optional simultaneous Th-Ar arc injection, or the inclusion of an iodine cell in the beam. The LR mode has unsliced 500µm fibres and makes provision for nod-and-shuffle for improved background subtraction. The MR mode also uses 500µm fibres, while the HR and HS fibres are 350µm. The latter three modes employ modified Bowen-Walraven image-slicers to subdivide each fibre into three slices. All but the High Stability bench is sealed within a vacuum tank, which itself is enclosed in an interlocking Styrostone enclosure, to insulate the spectrograph against temperature and atmospheric pressure variations. The Fibre Instrument Feed (FIF) couples the four pairs of fibres to the telescope focal plane and allows the selection of the appropriate fibre pair for a given mode, and adjustment of the fibre separation to optimally position the sky fibre. The HRS employs a photomultiplier tube for an exposure meter and has a dedicated auto-guider attached to the FIF. We report here on the commissioning results and overall instrument performance since achieving first light on 28 September 2013.

Keywords: Southern African Large Telescope, SALT, High Resolution Spectrograph, HRS, fibre-fed, échelle, Fibre Instrument Feed, FIF

1. INTRODUCTION

1.1 The Southern African Large Telescope (SALT)¹⁻⁶

The primary mirror of SALT consists of 91 spherically figured hexagonal 1m segments. The telescope is free to rotate in azimuth, but the elevation axis of the structure is fixed at 37° from the zenith. A tracker assembly at prime focus then moves about all six translational and rotational axes in order to track an object as it travels across the annulus of accessible sky. SALT is thus able to follow celestial targets for between one and three hours, depending on their declination. Consequently, observations are entirely queue-scheduled to make optimal use of targets' limited visibility windows. Access to observing time is limited to members of the SALT Consortium, which includes various groups distributed across seven partner countries.

The Tracker carries the Payload which includes the four-mirror Spherical Aberration Corrector⁷⁻¹² (the secondary optics that remove aberrations introduced by the spherical primary) and SALT's two first-light instruments: the acquisition and imaging camera (SALTICAM), and the multi-purpose low-resolution spectrograph (the Robert Stobie Spectrograph, RSS). An additional fold mirror in the Payload feeds a third focus, reserved for the final first generation instrument – a fibre-fed high resolution spectrograph, the HRS. Here the Fibre Instrument Feed (FIF) provides the interface for the 50m long fibre cable that conducts the light to the spectrometer room below the telescope, where the HRS is situated.

* lisa@sao.ac.za

1.2 The SALT High Resolution Spectrograph (HRS)

SALT HRS¹³⁻¹⁵ is an efficient fibre-fed, single-object spectrograph of a dual channel, ‘white pupil’ design. The instrument’s parabolic primary mirror thus acts to collimate light onto the R4 échelle grating (blaze angle $\theta_B = 76^\circ$), and also to focus dispersed light to an intermediate focus. A dichroic beam-splitter then separates the dispersed light into two separate spectral channels (370-555nm and 555-890nm). Spherical pupil mirrors transfer the separated beams via a fold mirror to two wavelength-specific volume-phase holographic gratings (VPHGs) used as cross-dispersers. The cross-dispersed spectra are then imaged by two fully dioptric camera systems onto optimized CCD detectors. A single $2k \times 4k$ CCD is sufficient to capture all of the blue orders, while a $4k \times 4k$, fringe-suppressing deep-depletion CCD, is used for the red camera. Complete free spectral ranges are covered by both the blue and red arms. Fig. 1 shows the optical layout of the spectrograph and Fig. 2 is a photograph of the échelle that consists of two identical $214\text{mm} \times 400\text{mm}$ gratings on a single Zerodur substrate.

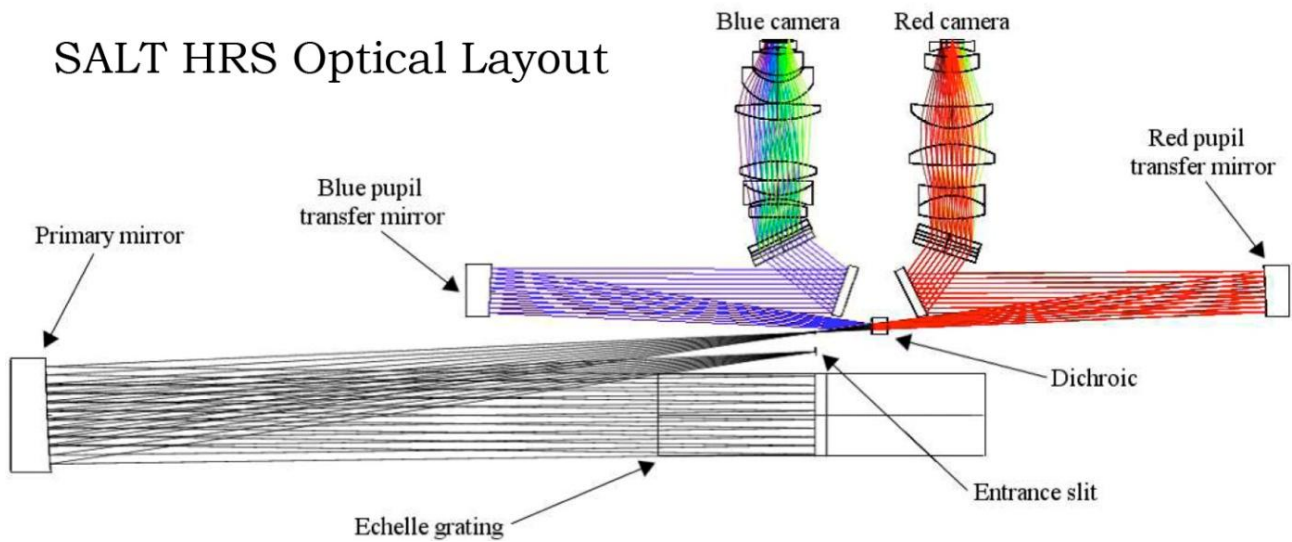


Figure 1. The optical layout of the SALT HRS (excluding the fore-optics), showing the white pupil design and the two channels optimized for blue (370-555 nm) and red (555-890 nm) wavelength ranges.

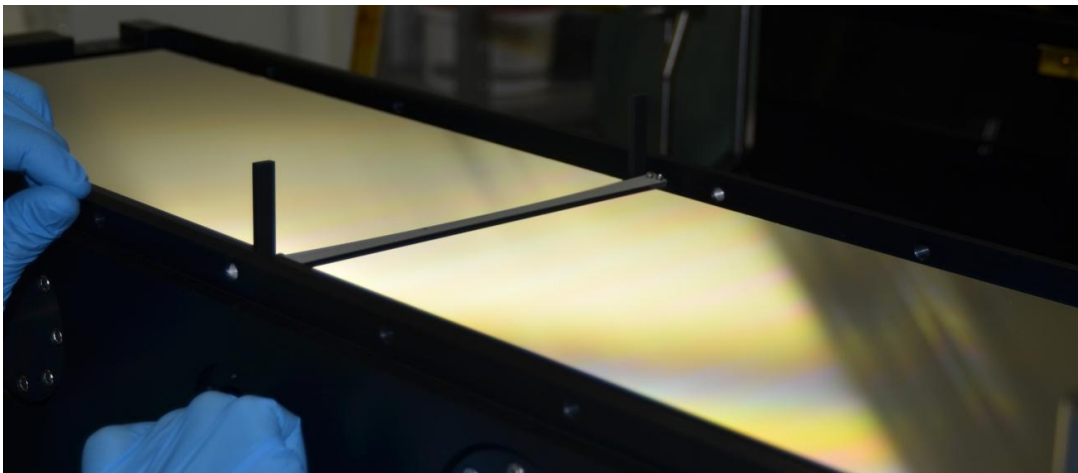


Figure 2. The physical scale of SALT HRS is perhaps best conveyed by the fact that the échelle grating weighs roughly as much as individual members of the instrument team! The narrow, spherically-figured pick-off mirror for the exposure meter can be seen in the centre of the grating, positioned in the dead space between the two sections of the échelle mosaic. The optical surface of the mirror is pointing to the left in this image.

Much of the optical design for the HRS¹⁶ was provided by the University of Canterbury in New Zealand, as their in-kind contribution to join the SALT consortium. Remaining design work and construction of the instrument began at Durham University's Centre for Advanced Instrumentation¹⁷ in late-2007. Installation and integration on site at SALT was carried out during September 2013 and first light was achieved on 28th September. This was followed by a period of Science Commissioning before SALT partners were invited to submit HRS Science Verification proposals. These observations were undertaken on a shared-risk basis (and thus not charged to SALT partner time allocations) and the instrument began delivering fully-charged science observations in May 2014. In this paper we present results obtained during the Commissioning and Science Verification phases that demonstrate the instrument's performance.

2. SALT HRS MODES

The fibre bundle for the HRS consists of 16 large, 500 μ m and 350 μ m diameter (2.2 and 1.6 arcsec on-sky, respectively), *PolyMicro Technologies FBP* broad spectrum step-index fibres. These core sizes were chosen to accommodate the relatively poor median seeing conditions at SALT. Each of the instrument's four modes (Low, Medium and High Resolution, and High Stability) has four fibres, one for the source (star), one for the background (sky) and spares for these (see Fig. 3). Three of the four fibre pairs (all but the LR mode) feed modified Bowen-Walraven image-slicers that reformat the fibre image into a narrow slit to improve the resolution. The modification to the slicer optics allows the star and sky fibres to be sliced simultaneously and to end up with identical optical path lengths through the slicing elements. The resolving powers for the various modes are: \sim 15000 for the unsliced 500 μ m fibres (LR), \sim 40000 for the sliced 500 μ m fibres (MR) and \sim 65000 for the sliced 350 μ m fibres (HR and HS).

2.1 Low Resolution (LR)

The lowest resolving-power, R \sim 15000 configuration should be seen as a specialist mode. This offers the same fibre input diameter as the R \sim 40000 mode (500 μ m), but with two beneficial differences: nominally 1.4 \times higher throughput because the fibre output is not image-sliced (hence the coarser resolution), and the opportunity to use nod-and-shuffle for improved sky subtraction. The nod-and-shuffle operation samples two different sky fields on either side of the target, for half of the total exposure time in each case. It ensures that object and sky spectra can be extracted from the same pixels on the CCD. In addition, the starlight falls on two different regions of the CCD (corresponding to the two fibre positions) and hence benefits from a $\sqrt{2}$ reduction in the impact of residual flat-field noise, but without an increase in read-noise. This improvement in sky sampling and reduction in flat-field residuals will benefit observations of the faintest targets requiring the lowest resolving power. Examples where the lowest resolving power may be tolerable and where the improved background sampling might be beneficial include spectroscopy of diffuse interstellar bands against lines of sight to distant stars or quasars, and molecular band analyses of stars in Local Group galaxies.

2.2 Medium Resolution (MR)

The R \sim 40000 mode is expected to be the most commonly used SALT HRS mode. It has adequately high resolving power for many projects, but with a larger fibre diameter and thus potentially better seeing-related throughput than the R \sim 65000 mode. Studies of objects whose intrinsic line widths are broader than two resolution elements of the R \sim 65000 mode, such as rotating stars (e.g. most O and B stars), stars in which the Balmer line strength measurements are the principal aims, and studies of molecular bands at medium resolution will be well suited to this mode.

2.3 High Resolution (HR)

The R \sim 65000 mode is likely to be selected for projects involving line profile variations when investigating stellar atmosphere dynamics, resolving closely spaced lines, or in exploring absorbing structures in the interstellar or intergalactic medium at the highest velocity resolution. Studies that benefit from fine sampling of stellar line profiles, such as the most precise radial velocity work, will also utilize this resolving power. However, given that the wavelength stability of the instrument as a whole is much higher than in traditional non-vacuum spectrographs, users may achieve adequate velocity accuracy even at R \sim 40000 due of the improved systematics compared to other spectrographs.

2.4 High Stability (HS)

The high stability mode is optimized for precision radial velocity measurements and is implemented at R \sim 65000, because of the importance of adequately sampling the line profiles in order to achieve sub-resolution-element accuracy

(an error of 0.5m/s corresponds to 10^{-4} of a resolution element!). The light path includes a permanent double-scrambler to improve the radial scrambling of the fibres and reduce the spectral shifts due to the star moving on the input face of the fibre. In this mode it is also possible to insert an iodine cell into the beam (both channels) to provide a superimposed set of wavelength reference lines in the 500-620nm range, or to illuminate the second (sky) fibre with an internal ThAr calibration source to obtain a simultaneous wavelength calibration. The efficiency of this mode is about half that of the normal high resolution mode and thus it would normally only be used where this level of wavelength stability is essential. Note that the simultaneous ThAr and iodine cell options may not be used at the same time.

Table 1. Summary of the four SALT HRS modes and the associated options.

Parameter	Low Resolution	Medium Resolution	High Resolution	High Stability
Fibre Diameter (μm)	500	500	350	350
Fibre Diameter (arcsec)	2.23	2.23	1.56	1.56
Slit Width (arcsec)	0.710	0.710	0.355	0.355
Image-Slicers	No	3 Slices	3 Slices	3 Slices
Blue Arm Resolving Power	15000	43000	65000	65000
Red Arm Resolving Power	14000	40000	74000	65000
Blue Transmission (% total @ 460nm)*	12	7	7	4
Red Transmission (% total @ 625nm)*	19	11	12	6
Fibre Mode Scrambling	No	No	No	Permanent
Nod and Shuffle	Optional	No	No	No
Iodine Cell**	No	No	No	Optional**
Simultaneous ThAr**	No	No	No	Optional**
Total Photon Count***	Yes	Yes	Yes	Yes

* These efficiency values are the as-measured 'end-to-end' throughput measurements for the spectrograph as a whole.

** Note that the Iodine Cell and Simultaneous ThAr feed cannot be used at the same time.

*** From the exposure meter (not available when using the Simultaneous ThAr feed in the HS mode)

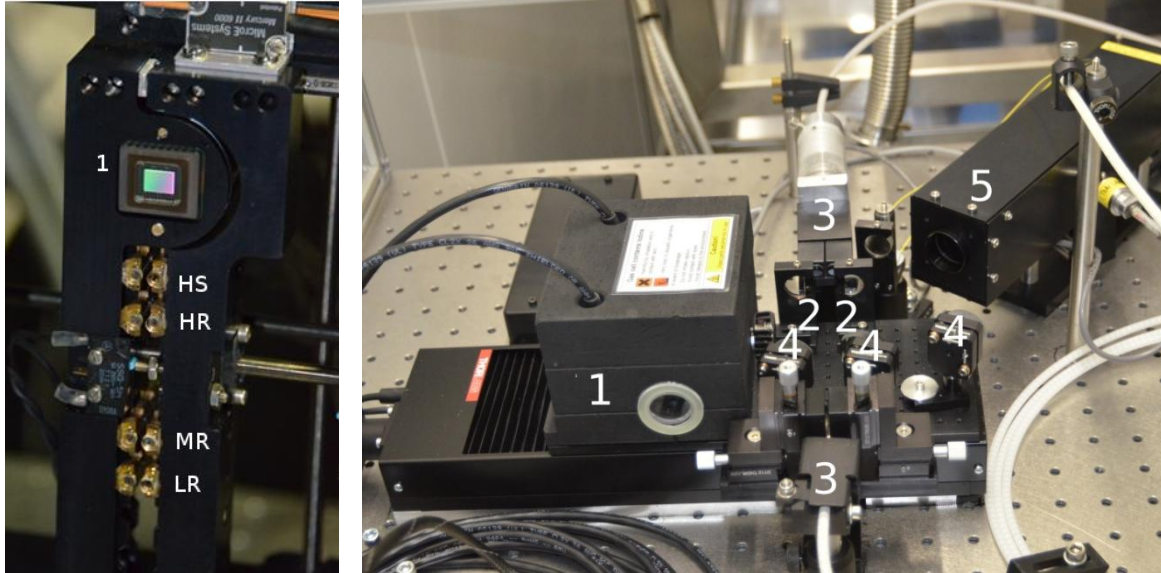


Figure 3. Left: the Fibre Instrument Feed with its acquisition camera (1) and the fibre pairs for the modes (HS, HR, MR and LR from top to bottom, star fibres on the left and sky fibres on the right). Right: the High Stability bench showing the iodine cell (1), the double-scrambler (2) gap in the HS fibres (3) and the fold mirrors (4) to direct light from the ThAr lamp (5) into the fibres.

3. INSTRUMENT PERFORMANCE

3.1 Throughput

End-to-end instrument throughput measurements were made for each mode (from the input ends of the fibres to the CCDs) prior to the fibre cable being routed up to the Payload. This was done using four narrow-band LEDs with peak wavelengths at 460nm and 505nm (for the blue channel) and 591nm and 625nm for the red channel. Each fibre input was illuminated using a small ($\sim 50\mu\text{m}$) spot at F/4.2, to simulate the output focal ratio of the telescope. The total input flux was measured using a calibrated photodiode and the LEDs were powered using a stabilized current source to ensure that the illumination remained constant to $\sim 1\text{-}2\%$ during the measurements (this was verified over the course of hours).

Since the bandpass of the LEDs is much greater than one spectrograph order, the detected signal on the CCDs was measured using an aperture large enough to capture most of the light in the cross-dispersed spectrum. The detected signal was corrected for background and converted to electrons using the measured gains for the blue and red chips. The measurements of the integrated signal were found to be repeatable to $\sim 2\%$ for different aperture sizes and background corrections. The number of incident photons was then estimated from the supplied photodiode calibration curve (W/A) at the mean wavelength of the diode, using an energy per photon calculated at the peak diode wavelength. Since the diode absolute calibration varies approximately linearly with wavelength across the LED spectrum (and the energy per photon varies inversely with wavelength), adopting a mean value should introduce negligible errors ($< 1\%$). Including all known sources of error (scattered light, diffraction) we estimate that the measurements are accurate to 5% of their absolute value. Measurements were taken for both 'star' and 'sky' fibres in all four modes and the efficiency data are plotted as a function of wavelength in Fig. 4 below.

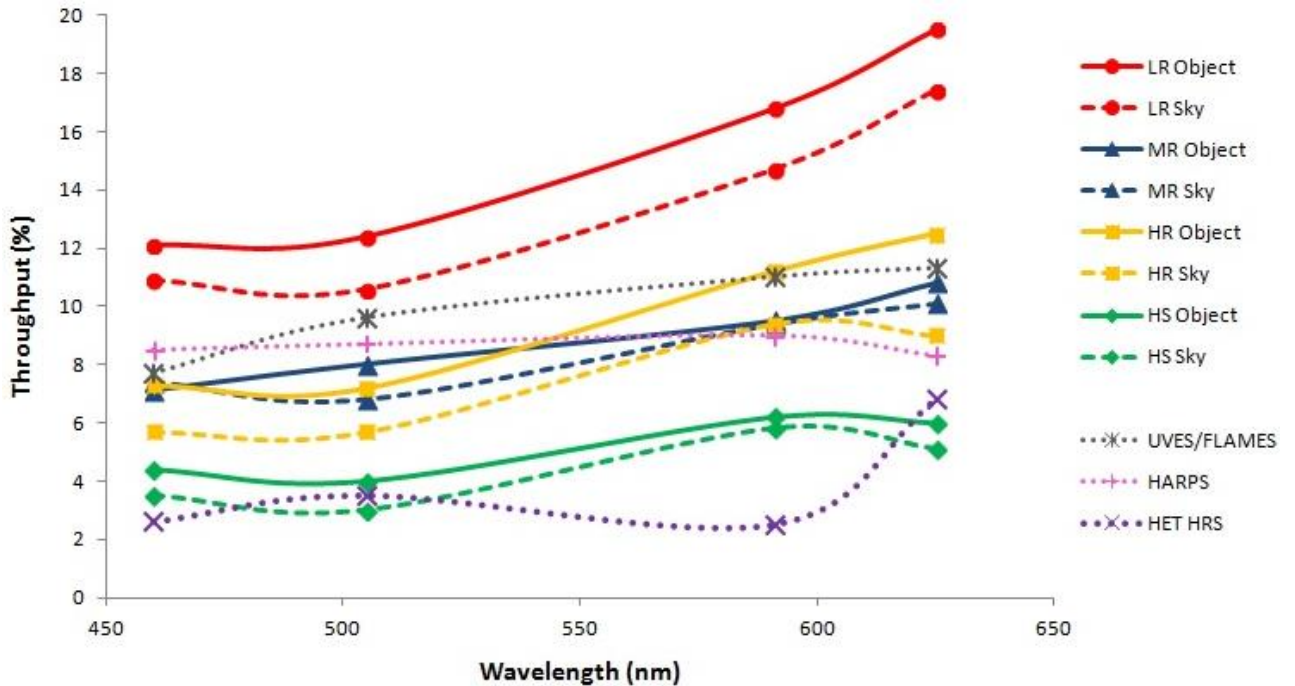


Figure 4. Fibre-input to CCD throughput measurements for the various HRS modes. Solid lines indicate star fibres while dashed lines represent the sky fibres. Dotted lines are estimates derived from the exposure time calculators for other high resolution spectrographs (UVES, HARPS and HET HRS) for comparison.

We have also included throughput estimates for three comparable fibre-fed échelle systems: HET HRS, FLAMES/UVES¹⁸ (the fibre feed to UVES from FLAMES) and HARPS¹⁹ in Fig. 4. These are not actual laboratory measurements, but were taken from the various exposure time calculators (ETCs) provided for these instruments, by assuming no entrance slit losses (0 arcsec seeing) and correcting where necessary for standard atmospheric (0.83-0.91) and mirror reflectivity (0.92 per surface) transmission (the ETCs generally include the telescope and atmospheric losses).

The MR and HR mode efficiencies would be expected to be very similar (as observed) as the optical layout is almost the same, and the benefits of the larger fibres in the MR mode are not reflected in this particular test (i.e. there is no atmospheric seeing). The HS mode transmission is somewhat lower, as expected from the double-scrambler, although these measurements were made before the final optimization of the double-scrambler alignment was made and are likely to be underestimates of the true efficiency. These measurements of the four fibre pairs led to those with the highest transmission being selected as the default object fibres for each mode. Note that the differences between fibres at the level observed are typical, HARPS quotes a difference of 30% in the relative transmission of their star-sky fibre pair.

A separate measurement was also made of the fibre cable transmission losses at 460nm, using the same setup on the HS fibres, by measuring the output in the gap between the double-scrambler lenses. The measured transmissions were 72.4% for the HS sky fibre and 78.9% for the HS star fibre. The manufacturer lists the attenuation for this type of fibre to be 26 dB/km at this wavelength, so for a 42m length of cable this gives 22% transmission loss at 460nm. Adding in 1% Fresnel losses at the fibre input and output (the output is optically bonded to the double-scrambler lens, so there is only one AR-coated air-glass surface at each end), the predicted throughput would be 76%. This is in good agreement with the average measured transmission (75.6%).

Reliable on-sky throughput measurements require photometric conditions, good seeing, a well aligned SALT primary mirror and the cooperation of a number of telescope and instrument sub-systems. The HRS Exposure Time Calculator (ETC) was used to predict fluxes from the HRS for a radial velocity standard star (HD157881, a K7 dwarf with an effective temperature of 4020K, a surface gravity of 4.50 and a V-band magnitude of 8.1) that was observed under these favourable conditions. The ETC predictions could then be compared with spectra obtained while the Sutherland seeing monitor reported 1.4 arcsec seeing and the HRS auto-guider measured a FWHM = 1.6 arcsec on the guide star. Fig. 5 shows the comparison between the measured S/N ratio and the prediction from the ETC for each channel, assuming a Kurucz model with an effective temperature of 4000K. We also show the prediction (green dashed line) using the VLT ETC for UVES/FLAMES (R~47000), but assuming seeing of FWHM = 0.75 arcsec. The FLAMES fibres are 1.0 arcsec diameter and 55 metres long so the aperture losses are equivalent to using a 2.2 arcsec diameter fibre in FWHM = 1.5 arcsec conditions with SALT HRS (and also fairly reflects the different intrinsic seeing at the two sites).

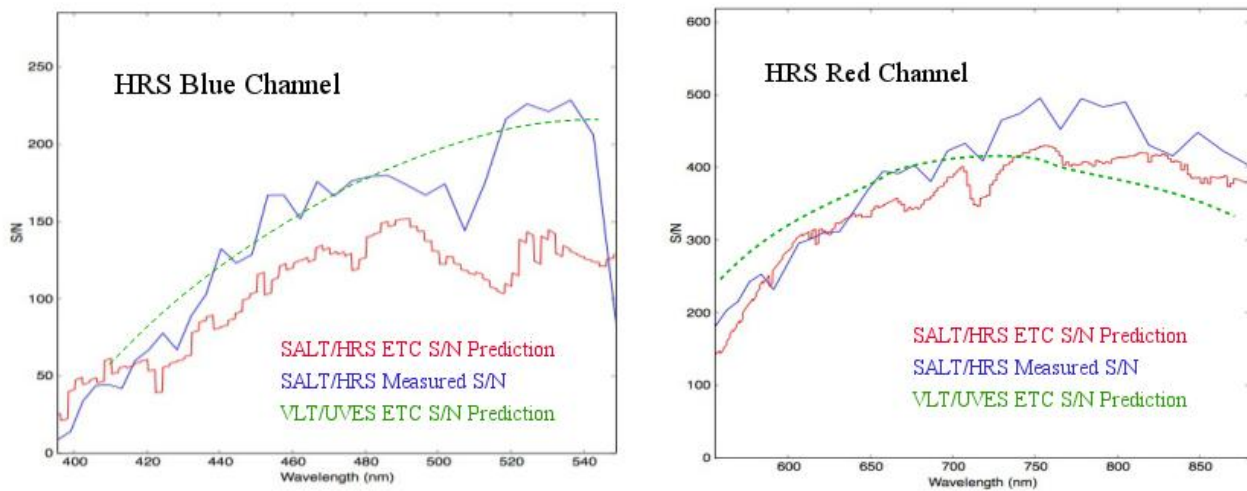


Figure 5. Comparisons between the SALT HRS ETC S/N predictions and MR mode spectra of a radial velocity standard star obtained under photometric conditions with 1.5 arcsec seeing and a well-aligned primary mirror. The blue channel is shown on the left and the red on the right. The dashed line shows the VLT/UVES ETC prediction for R~47000 and 0.75 arcsec seeing.

The SALT HRS efficiencies currently encoded into the ETC are close for the blue channel, but are ~10% too high for the red channel. We note that the Pickles stellar models would produce better predictions than the Kurucz models (e.g. the strong absorption feature at 710nm in the ETC curve is due to a failure of the Kurucz models) and so these will be incorporated into the HRS ETC. The absorption dip in the HRS spectrum at 770nm is due to the telluric A-band.

3.2 Stability

Stability is critical for high resolution spectrographs to be competitive. To this end, the SALT HRS optical components are mounted on an optical bench contained within a steel vacuum tank that is held at a pressure of 0.05 mBar. The instrument is thus well isolated from the destabilizing effects of temperature and atmospheric pressure variations. The tank rests on pneumatic isolators to minimize vibrations and is bricked inside a Stryrostone enclosure for additional thermal insulation. The temperature of the instrument room is also actively controlled to within a few tenths of a degree Celsius, while the tank temperature is fine-tuned by a heating wire bonded to the outer surface of the tank. Numerous temperature sensors constantly monitor the main optical components, the bench, the tank and the air inside and outside the thermal enclosure. The wavelength stability of the instrument is monitored with regular internal ThAr arc exposures.



Figure 6. Left: HRS inside its insulated enclosure (1) in the spectrometer room below SALT. With the side door panel removed, one can see the vacuum tank (2), the High Stability bench (3), the blue and red cameras (4), the insulation on the floor (5) and the instrument PI (6). Right: inside the HRS room, with the Styrostone (1) thermal enclosure only partly built up around the tank. The various cable feed-throughs (2), the tank heating wire (3), the vacuum hose (4) and the exposure meter (5) can also be seen.

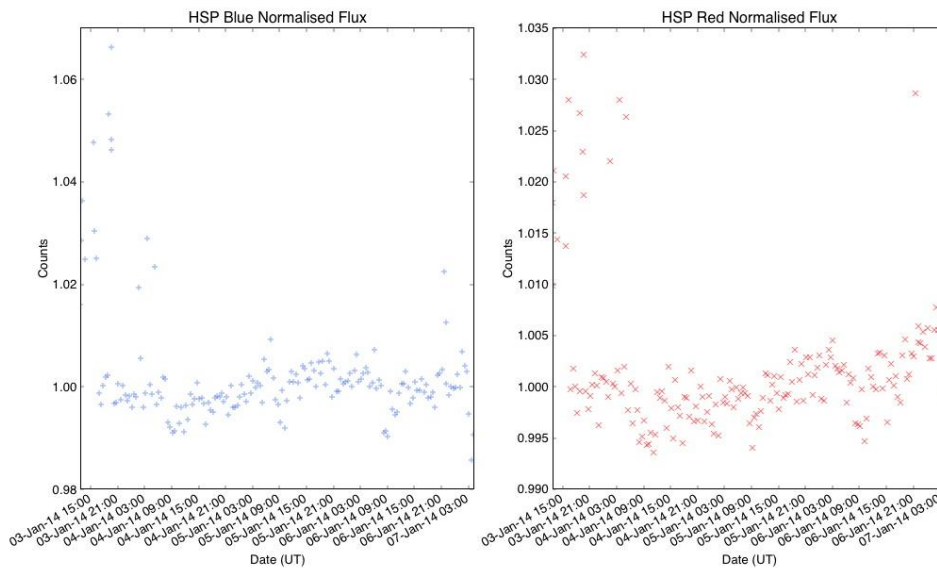


Figure 7. Normalised flux measurements of the internal ThAr calibration lamp for the blue (left) and red (right) channels over a 3.5 day interval, showing the line stability as the system settled down after an air-conditioning glitch. The system meets the stability specification of 10% (rms) over a 12 hour period.

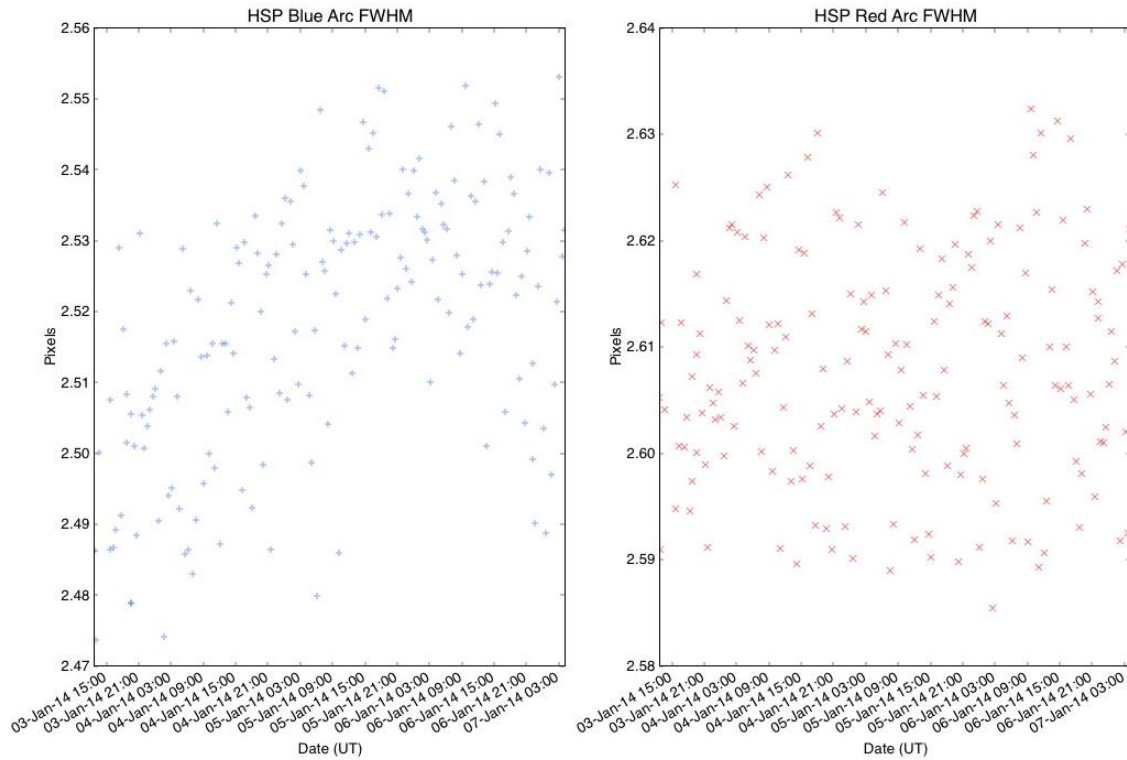


Figure 8. Line width (FWHM) measurements of the internal ThAr calibration lamp for the blue (left) and red (right) channels over a 3.5 day interval. The system meets the stability specification of 1% (rms) over a 12 hour period.

3.3 Spectral Resolution

The spectral resolution for the LR, MR and HR modes was measured on the telescope using the SALT calibration system's ThAr arc to illuminate both fibres. Because of the extreme faintness of this source, several long exposure arcs (typically 1800s each) were median-combined to improve the S/N. For the HS mode it was possible to use the internal ThAr arc lamp on the high stability bench. This is considerably more efficient and so the exposure times were only 10s.

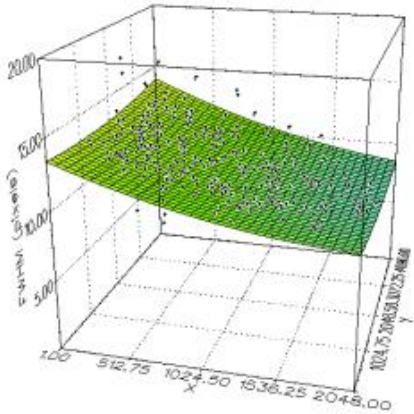
The arc lines were detected using SExtractor²⁰ and the spectral line widths were measured using a Python Gaussian-fitting script. Individual FWHM measurements, as a function of position on the detector, were fitted using a quadratic surface to look for systematic effects associated with field curvature and anamorphic magnification. The median spectral resolutions for the blue and red channels were then calculated in 3×3 grids covering the two chips. A mean dispersion of 0.0032 nm/pixel and a central wavelength of 475nm were used for the blue channel, while a mean dispersion of 0.0043 nm/pixel and a central wavelength of 700nm were applied for the red channel. The surface plots for each mode and channel, and the corresponding median spectral resolutions, are shown in Figures 9 and 10 below, with the number of lines averaged for each measurement given in parentheses. The dominant effect causing the spectral resolution to change in the dispersion direction is the variation in anamorphic magnification from the échelle. This is most pronounced for the MR mode as those slits are offset the furthest from the optical axis of the collimator. It is also always more pronounced for the red channel with its more extended CCD.

Table 2. Specified and achieved resolving powers for the blue (left) and red (right) channels in the various modes.

Mode	Specification	Achieved
Low Resolution	12700 12700	15000 14000
Medium Resolution	33000 33600	43400 39600
High Resolution	58000 62300	66700 73700
High Stability	58000 62300	66900 64600

Blue Channel

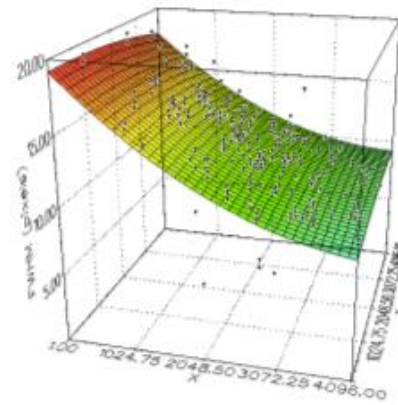
Low Resolution



	X₁	X₂	X₃	Y_{ave}
Y₁	12120 (48)	14850 (39)	17360 (11)	14777
Y₂	12480 (89)	14860 (71)	16910 (34)	14750
Y₃	12710 (35)	15260 (33)	16720 (7)	14897
X_{ave}	12437	14990	17000	

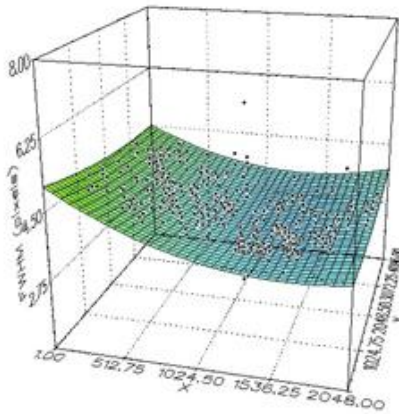
Red Channel

Low Resolution



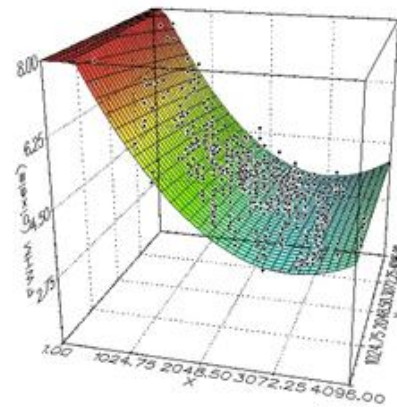
	X₁	X₂	X₃	Y_{ave}
Y₁	10440 (31)	13920 (57)	16080 (18)	13480
Y₂	11100 (38)	13480 (72)	16400 (35)	13660
Y₃	10300 (10)	14330 (34)	16380 (30)	13670
X_{ave}	10613	13910	16287	

Medium Resolution



	X₁	X₂	X₃	Y_{ave}
Y₁	36930 (51)	42850 (28)	45250 (15)	41677
Y₂	37730 (69)	43260 (97)	45610 (61)	42200
Y₃	36330 (29)	44170 (42)	45320 (18)	41940
X_{ave}	37000	43427	45393	

Medium Resolution

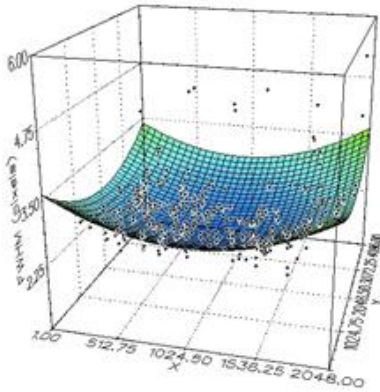


	X₁	X₂	X₃	Y_{ave}
Y₁	29170 (40)	41800 (151)	47670 (40)	39547
Y₂	29220 (47)	39120 (183)	45830 (66)	38057
Y₃	26390 (11)	37890 (45)	46140 (58)	36807
X_{ave}	28260	39603	46547	

Figure 9. Resolving powers measured from ThAr arc lines distributed over 3x3 grids on blue (left) and red (right) channel images for the Low Resolution (top) and Medium Resolution (bottom) HRS modes. Values in parentheses indicate the number of arc lines included in each measurement. See the end of Section 3.3 for details.

Blue Channel

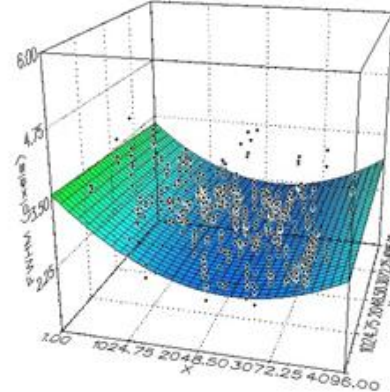
High Resolution



	X₁	X₂	X₃	Y_{ave}
Y₁	63980 (55)	69110 (34)	60660 (18)	64583
Y₂	61380 (117)	67770 (118)	61950 (51)	63700
Y₃	63230 (48)	63230 (22)	52890 (18)	59783
X_{ave}	62863	66703	58500	

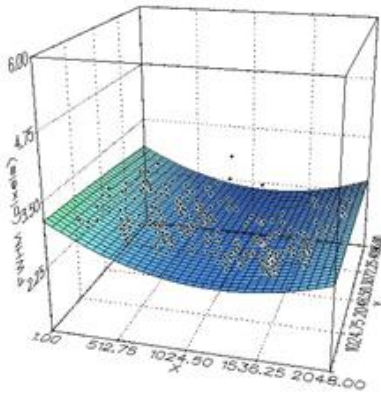
Red Channel

High Resolution



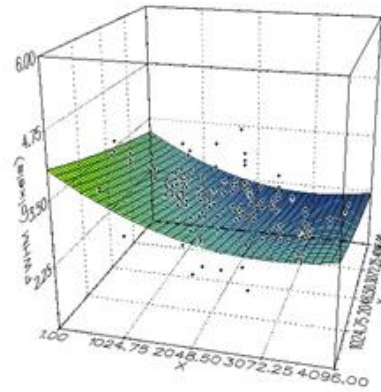
	X₁	X₂	X₃	Y_{ave}
Y₁	63210 (80)	74790 (132)	68220 (27)	68740
Y₂	62080 (94)	71960 (141)	80760 (41)	71600
Y₃	59060 (17)	74310 (54)	72420 (57)	68597
X_{ave}	61450	73687	73800	

High Stability



	X₁	X₂	X₃	Y_{ave}
Y₁	59010(12)	70370 (13)	64070 (5)	64483
Y₂	56930 (47)	65420 (54)	64970 (30)	62440
Y₃	58140 (27)	64810 (30)	66740 (29)	63230
X_{ave}	58027	66867	65260	

High Stability



	X₁	X₂	X₃	Y_{ave}
Y₁	60830 (20)	72200 (39)	74040 (7)	69023
Y₂	54320 (33)	60830 (39)	69540 (22)	61563
Y₃	46460 (4)	60610 (17)	69950 (6)	59007
X_{ave}	53870	64547	69963	

Figure 10. Resolving powers measured from ThAr arc lines distributed over 3x3 grids on blue (left) and red (right) channel images for the High Resolution (top) and High Stability (bottom) HRS modes. Values in parentheses indicate the number of arc lines included in each measurement. See the end of Section 3.3 for details.

4. SALT HRS OPERATIONS

As with the other SALT instruments, HRS proposals are written and submitted using the SALT Principal Investigator Proposal Tool (PIPT), in conjunction with the SALT HRS exposure time calculator. These proposals go into the Science Database where they are accessible to the SALT Astronomy Operations Team via the Web Manager. Active proposals are then subject to queue scheduling so that when a target becomes visible to SALT, the Observation Configuration System may be used to send the desired settings to the instrument. The HRS MMI is a LabVIEW graphical interface that is used to configure the instrument and run the procedures required to capture the data. The first phase of the HRS data reduction software is a Python/PyRAF based quick-look tool with a PyQt GUI that will allow the SALT Astronomer to assess data quality at the telescope. The data are then transferred to Cape Town for basic pipeline reduction the next day, before being made available to the PIs for download. A full HRS data pipeline will eventually be incorporated into the PySALT suite of data reduction and analysis packages.

SALT HRS offers a variety of detector configurations. The CCDs can be read out at either 400 kHz or 1000 kHz (with read noise of 3.6 and 4.7 e^- RMS, respectively, in the red; and 4.2 and 5.8 e^- RMS in the blue), through either single or multiple readout amplifiers (two in the case of the blue channel and four in the red). Binning choices include 1×1 , 2×2 , 3×3 , 9×9 and 3×1 , the latter with binning in the spatial direction only. Exposure times need not be the same for the red and blue channels. The detectors do, however, have to be read out sequentially and so even if the exposure times are equal, it will still take approximately 50s to read out both chips and write the new files (for a set of unbinned frames). A windowed readout option has yet to be implemented, but will be made available in the future.

A custom-made pick-off mirror (a 200mm long sliver of aircraft-grade aluminium, diamond-turned to produce the required spherical figure on the ~ 2 mm wide optical surface) is mounted in the 16mm wide gap between the two identical sections of the échelle grating mosaic. Starlight that would otherwise be wasted is thus fed to a photomultiplier tube (PMT) that serves as an exposure meter (EM). This allows the observer to monitor the progress of an exposure and adapt accordingly to varying observing conditions. The EM reports the total counts recorded by the PMT, allowing the mean count and the flux-weighted mid-point of the exposure to be calculated. The latter is particularly important for radial velocity studies where a precise correction for the Earth's orbital motion needs to be applied. The EM is suitable for targets ranging in brightness from $V \approx 3-14$ and is also useful for peaking up the fibre position during acquisition, as well as for monitoring the telescope focus through the course of the observation.

The two panels in Fig. 11 illustrate the spectral formats for the red and blue cameras, including the orders, their blaze wavelengths and inter-order spacings, as well as the positions of various spectral features. Fig. 12 shows raw blue (left) and red (right) calibration frames for the different sliced modes. Both fibres are illuminated in all cases so the orders are paired. The images are HR twilight sky flats (top), MR SALT CalSys ThAr+Ar arcs (centre) and HS flat-fields with the iodine cell in the beam (bottom), superimposing a dense forest of absorption features on the spectra.

The SALT calibration system will soon be upgraded substantially and this will greatly simplify HRS operations. The current system has made it impractical to take arcs during the night, or even to do so regularly during the daytime. Although the instrument's intrinsic stability reduces the need for daily calibrations, an appropriate schedule for taking arcs and flat-fields will be established once the new SALT CalSys is in operation (likely within the next few months). Sets of 11 bias frames are currently taken each night while sky flats are obtained on a \sim monthly basis. Internal ThAr arcs will continue to be taken daily to monitor the stability of the instrument, particularly once the remaining thermal insulation issues have been addressed. CalSys flats use a quartz/tungsten/halogen source with a 'Clear-UV' filter to help balance the flux distribution while CalSys arcs currently include both a ThAr and an Ar lamp. Radial velocity standard star observations will continue to be made during twilight and made available to all HRS PIs.

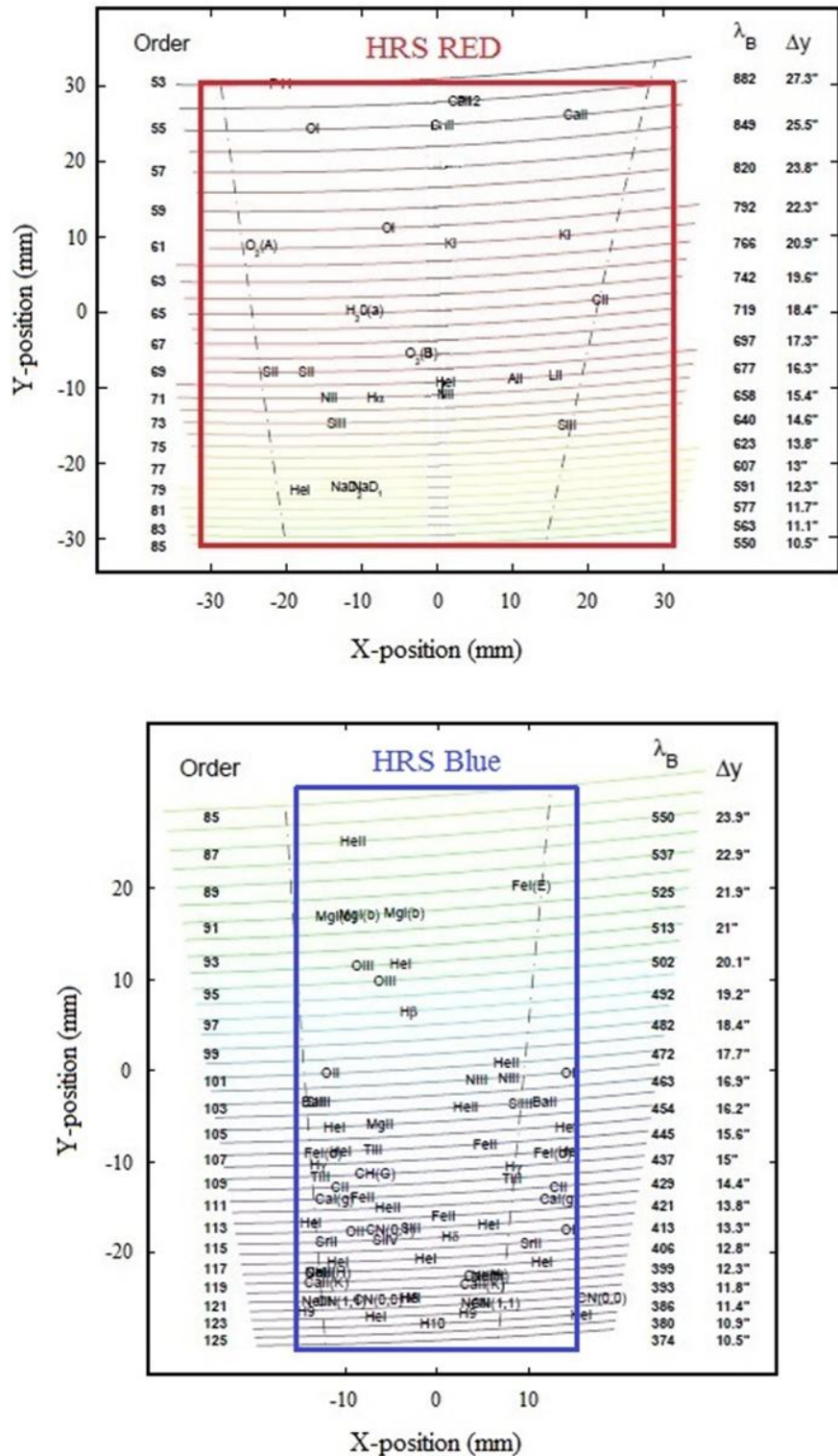


Figure 11. The simulated spectral formats of the SALT HRS red (top) and blue (bottom) channels, showing the order numbers (m), the blaze wavelength (λ_B) of each order, the inter-order spacing (Δy) and the position of some commonly studied spectral lines. The dashed lines indicate the limits corresponding to one free spectral range in each order. Wavelengths increase from left to right and bottom to top in each panel.

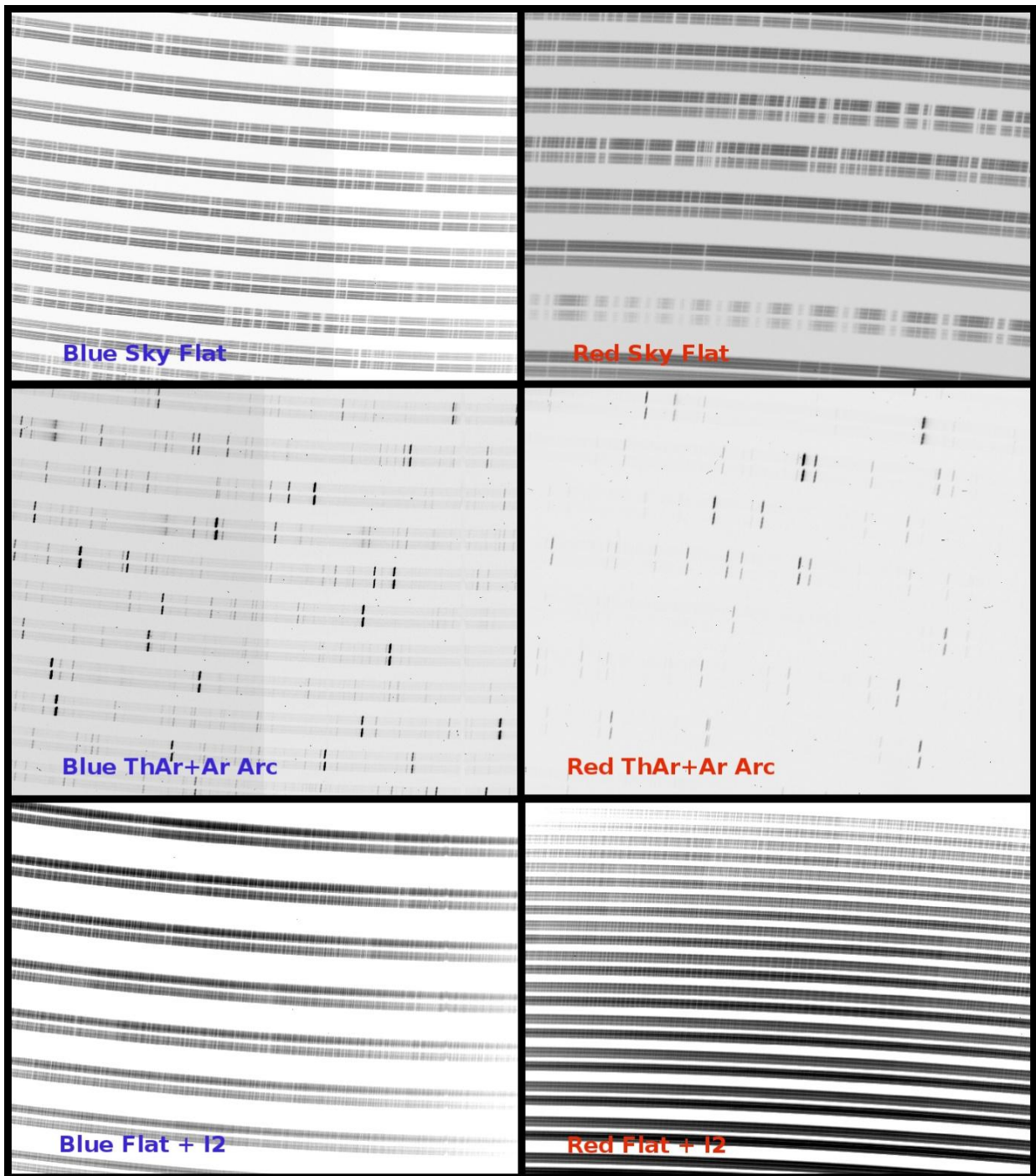


Figure 12. Raw HRS calibration frames, blue on the left and red on the right. From top to bottom these are: twilight sky flats, SALT CalSys ThAr+Ar arcs and CalSys flat-field images taken with the iodine cell in the beam, superimposing a dense forest of iodine absorption lines on the 500-620nm region of the two cameras.

5. SUMMARY

The HRS was delivered to SALT on 3 September 2013. The 40 foot shipping container and 15 airfreight crates were unpacked and the instrument reassembled and integrated into the facility. This process was documented daily on the SALT Astronomy Blog²¹ during the month of September. First light on 28 September was followed by commissioning and science verification observations. The instrument meets (or exceeds) specification in terms of spectral resolution, throughput and stability and compares favourably with similar spectrographs such as UVES on the VLT. SALT HRS is now fully operational and available to the SALT community.

REFERENCES

- [1] Stobie, R., Meiring, J. G., Buckley, D. A. H., “Design of the Southern African Large Telescope (SALT)”, Proc. SPIE 4003, 355 (2000).
- [2] Swat, A., O’Donoghue, D., Swiegers, J., Nel, L. and Buckley, D. A. H., “The optical design of the Southern African Large Telescope”, Proc. SPIE 4837, 564 (2003).
- [3] Buckley, D. A. H., Swart, G. P., Meiring, J. G., “Completion and commissioning of the Southern African Large Telescope”, Proc. SPIE 6267, 564 (2003).
- [4] Meiring, J. G., Buckley, D. A. H., “Southern African Large Telescope (SALT) project, progress and status after 4 years”, Proc. SPIE 5489, 592 (2004).
- [5] O’Donoghue, D. et al., “First science with the Southern African Large Telescope: peering at the accreting polar caps of the eclipsing polar SDSS J015543.40+002807.2”, Mon. Not. R. Astr. Soc., 372, 151 (2006).
- [6] <http://www.salt.ac.za>
- [7] O’Donoghue, D., “Correction of spherical aberration in the Southern African Large Telescope (SALT)”, Proc. SPIE 4003, 363 (2000).
- [8] <http://www.salt.ac.za/iq/the-salt-image-quality-story>
- [9] <http://saltiqmission.blogspot.com>
- [10] O’Donoghue, D. E. et al., “The image quality of the Southern African Large Telescope (SALT)”, Proc. SPIE 7018, 32 (2008).
- [11] O’Donoghue, D. E., O’Connor, J. E., Crause, L. A., Strümpfer, F., Strydom, O. J., Brink, J. D., Sass, C., Wiid, E., Atad-Ettdgui, E., “Saving SALT: repairs to the spherical aberration corrector of the Southern African Large Telescope (SALT)”, Proc. SPIE 7739, 21 (2010).
- [12] Crause, L. A., O’Donoghue, D. E., O’Connor, J. E., Strümpfer, F., Strydom, O. J., Sass, C., du Plessis, C., Wiid, E., Love, J., Brink, J. D., Wilkinson, M., Coetzee, C., “A happy conclusion to the SALT image quality saga”, Proc. SPIE 8444, 8444I (2012).
- [13] Bramall, D. G., Sharples, R., Tyas, L., Schmoll, J., Clark, P., Luke, P., Looker, N., Dipper, N., Ryan, S., Buckley, D. A. H., Brink, J., Barnes, S. I., “The SALT HRS spectrograph: final design, instrument capabilities, and operational modes”, Proc. SPIE 7735, 77354F (2010).
- [14] Bramall, D. G., Schmoll, J., Tyas, L. M. G., Clark, P., Younger, E., Sharples, R. M., Dipper, N., Ryan, S. G., Buckley, D. A. H., Brink, J., “The SALT HRS spectrograph: instrument integration and laboratory test results”, Proc. SPIE 8446, 84460A (2012)
- [15] Tyas, L. M. G., “The SALT HRS Spectrograph” (2011) - PhD Thesis
- [16] Barnes, S., Cottrell, P., Albrow, M., Frost, N., Graham, G., Kershaw, G., Ritchie, R., Jones, D., Sharples, R., Bramall, D., Schmoll, J., Luke, P., Clark, P., Tyas, L., Buckley, D., Brink, J., “Optical design of the Southern African Large Telescope High Resolution Spectrograph: SALT HRS”, Proc. SPIE 7014, 70140K (2008).
- [17] <https://www.dur.ac.uk/cfai/>
- [18] Dekker, H., D’Odorico, S., Kaufer, A., Delabre, B., Kotzlowski, H., “Design, construction and performance of UVES, the échelle spectrograph for the UT2 Kueyen Telescope at the ESO Paranal Observatory”, Proc. SPIE 4008, 534-545 (2000).
- [19] Pepe, F., Mayor, M., Queloz, D., Udry, S., Delabre, B., Kohler, D., Lacroix, D., Sivan, J., Benz, W., Bertaux, J.: “HARPS: a new high-resolution spectrograph for the search extrasolar planets”, Proc. SPIE 4008, 582 (2000).
- [20] Bertin, E., Arnouts, S., “SExtractor: Software for source extraction”, Astronomy & Astrophysics Supplement 117, 393 (1996).
- [21] <http://saltastro.blogspot.com/2013/09/welcome-hrs-airfreight-including.html>